Probing the electron-phonon coupling in ozone-doped graphene by Raman spectroscopy

F. Alzina,[1,*] H. Tao,[1,†] J. Moser,[1] Y. García,[1] A. Bachtold,[1] and C. M. Sotomayor-Torres[1,2]
[1]*CIN2 (Institut Català de Nanotecnologia-Consejo Superior de Investigaciones Científicas), Campus UAB, 08193 Bellaterra, Spain*
[2]*Institució Catalana de Recerca i Estudis Avançats (ICREA), 08010 Barcelona, Spain*
(Received 14 May 2010; revised manuscript received 12 July 2010; published 23 August 2010)

We have investigated the effects of ozone treatment on graphene by Raman scattering. Sequential ozone short-exposure cycles resulted in increasing the *p*-doping levels as inferred from the blueshift of the 2*D* and *G* peak frequencies, without introducing significant disorder. The two-phonon 2*D* and 2*D*′ Raman peak intensities show a significant decrease while, on the contrary, the one-phonon *G* Raman peak intensity remains constant for the whole exposure process. The former reflects the dynamics of the photoexcited electrons (holes) and, specifically, the increase in the electron-electron-scattering rate with doping. From the ratio of 2*D* to 2*D*′ intensities, which remains constant with doping, we could extract the ratio of electron-phonon coupling parameters. This ratio is found independent on the number of layers up to ten layers. Moreover, the rate of decrease in 2*D* and 2*D*′ intensities with doping was found to slowdown inversely proportional to the number of graphene layers, revealing the increase in the electron-electron collision probability.

DOI: 10.1103/PhysRevB.82.075422 PACS number(s): 63.20.kd, 63.22.Rc, 78.30.−j, 78.67.Wj

I. INTRODUCTION

Graphene linear carrier dispersion in the vicinity of two inequivalent points ($\mathbf{K},\mathbf{K}'$) of the Brillouin zone creates the conditions for the occurrence of unusual effects on the dynamics of both electrons (holes) and phonons, which are related to the electron-phonon (*e-ph*) interaction.[1–3] In graphene, doping can be tuned by means of the field effect, i.e., electric charge induced by capacitive coupling.[4] Moreover, being a system entirely exposed to its environment, modification of the carrier concentration in graphene can follow from molecules adsorbed on the surface by charge transfer.[5,6] The control of the carrier concentration allows the study of electron-phonon coupling (EPC) effects since the *e-ph* interaction is directly modified by changing the Fermi-energy level. Raman-scattering measurements in field-effect devices showed the dependence of the *G* peak position and linewidth with doping, where *G* is the one-phonon mode at the Γ point, unveiling tunable optical phonon anomalies.[7–11] The possibility to monitor doping-oriented studies in graphene by Raman spectroscopy has provided the basis for a large range of application.[12–15]

Besides the effects of doping on the frequency and linewidth of the Raman *G* peak, the intensity of the 2*D* two-phonon signature, or the ratio of peak intensities $I(2D)/I(G)$, was found to decrease with increasing doping[9] and used as a tool to qualitatively establish the presence of charged impurities.[16,17] More recently, an understanding of how the two-phonon Raman peaks intensity depends on doping has been provided based on fully resonant processes[18,19] and their dependence on the *e-ph* and electron-electron (*e-e*) collision rates established. In Refs. 20 and 21, the *e-ph* scattering rate was not entirely obtained from experiments as the analysis of the 2*D* peak intensity requires the calculation of the *e-e* scattering rate.

Ozone treatment is considered as a promising route to enhance the otherwise weak chemical reactivity of graphitic structures.[22–24] The conductivity of carbon nanotubes (CNTs) was found to increase at low ozone dose or exposure time.[25,26] The proposed mechanism for this increase was the ozone adsorption on the CNT surface, which induces charge-transfer effects. At high ozone dose (or exposure time), the generation of structural modifications and defects seems to be the cause of a reduced conductivity.[26] In this paper we investigate the effects of sequential ozone treatment cycles on graphene flakes by analyzing the Raman spectrum. Our studies show that graphene displays similar changes with ozone as those reported in CNTs, i.e., *p*-type doping without introducing significant disorder at low exposure and different degrees of bond disruption and surface etching at high exposure. Here, we restrict our study to low exposure conditions and a full account on graphene oxidation by ozone will be published elsewhere.[27] Raman spectroscopy tracks the process of gradual *p* doping of the samples, as concluded from both the position and the intensity of the Raman peaks. From the latter we could determine the EPC for the phonon modes near the **K** point, and to monitor the *e-e* scattering contribution with increasing charge concentration as well as with the number of graphene layers. We found a good correlation between the rate of the intensity decrease upon doping and the number of graphene layers.

II. SAMPLES AND EXPERIMENTAL METHOD

Graphene sheets, prepared by micromechanical cleavage of highly ordered pyrolytic graphite (HOPG),[4] were deposited on Si wafers with 300 nm thick thermal silicon oxide. Ozone treatment of the samples was performed at room temperature with a Novascan UV-Ozone cleaning system. The ozone is produced in the cell by ultraviolet light irradiation of molecular oxygen (the initial oxygen pressure was of about 4 atm). The morphology of the graphene sheets was studied using a nanoscope atomic force microscope (AFM) in tapping mode. Micro-Raman measurements were carried out at room temperature in backscattering geometry using a T64000 Jobin-Yvon spectrometer with a cooled charge-coupled-device detector. In micro-Raman measurements the light was focused to a spot with diameter of about 1 μm

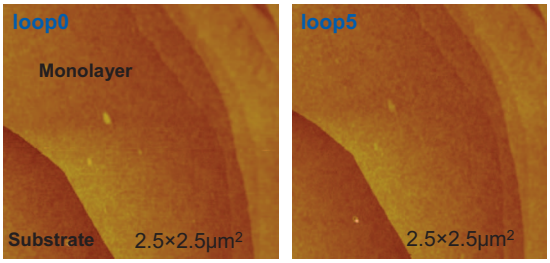

FIG. 1. (Color) AFM images obtained from the same graphene sheet before ozone treatment (loop 0) and after five exposure cycles to ozone (loop 5).

through a 100x objective. The 514.5 nm emission line of an Ar^+ laser was used for excitation with a typical power of only 120 μW, in order to prevent structural damage of the sample surface by the laser irradiation.[28] Raman peak lineshape and visible-light absorption were used to determine the number of layers.[29]

Graphene samples were placed on the ozone cleaner for cycles of fixed duration. After each exposure, samples were analyzed morphologically by AFM and by Raman spectroscopy. The exposure time of 2.5 min during each cycle ensures the graphene surface quality is preserved. In Fig. 1 AFM images taken from the same sample region before and after five exposure cycles [Fig. 1 (loop 0) and (loop 5), respectively] reveal smooth surfaces. Here, loop 0 refers to no exposure to ozone while loop n refers to a sample exposed to n consecutive loops. This observation differs from the irregular nucleation of the ozone-induced etching process that takes place at higher exposure times or temperature conditions than the used in this work.[23,27] Moreover, the structural disorder-related D peak is barely detected in the Raman spectra, which indicates that the density of defects in the graphene surface before and after the ozone exposure lies below the sensitivity of the Raman-scattering measurement.

III. RESULTS AND DISCUSSION

The Raman spectrum of graphitic structures shows common features, i.e., the main one-phonon G peak [cf. Fig. 2(a)], and defect-assisted one-phonon D and D' peaks, the expected frequencies of which are indicated by arrows in Fig. 2(a).[30] The G and D' peaks correspond to phonons at and near the Brillouin Γ point (E_g mode), respectively. The D peak comes from phonons near the $\boldsymbol{K}$ points (A_1 mode). Both D and D' peaks, which are evidence of intervalley and intravalley double-resonance processes, respectively, require defect scattering for their activation. Thus, these peaks are only detected when carbon planes present structural imperfections.[31–33]

The peaks denoted as $2D$ and $2D'$ in Fig. 2(b) are the second order of the D and D' peaks, respectively, involving two-phonon processes with opposite wave vectors, which do not require the presence of defects for their activation. The strongest and featureless $2D$ peak in monolayer graphene evolves to a structured lineshape as the number of layers increases, revealing the electronic band structure, which, in turn, depends on the number of stacked layers.[34]

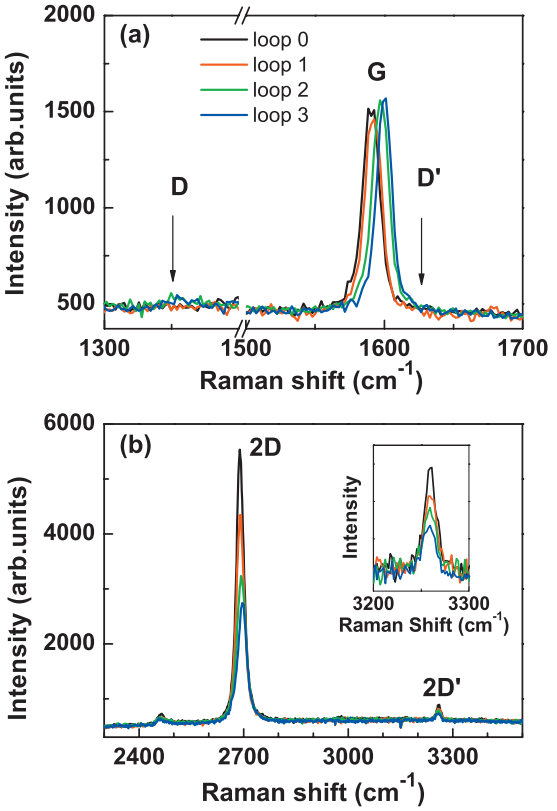

FIG. 2. (Color) (a) First- and (b) second-order Raman spectra of single-layer graphene taken from the pristine sample (loop 0) and after each exposure to ozone up to three cycles (loop 1 to loop 3). The inset shows the enlarged spectra in the spectral range of the $2D'$ Raman peak.

A. Second-order Raman peaks intensity

With increasing ozone exposure, the two-phonon $2D$ and $2D'$ Raman peak intensities show a significant decrease [see Fig. 2(b) and inset to Fig. 2(b)] while, in contrast, the one-phonon G Raman peak intensity remains unchanged with ozone doping.

The activation of $2D$ and $2D'$ peaks involves four-step processes where all the states are real, and require energy and momentum conservation at every elementary step, which means that both two-phonon Raman processes are fully resonant. As a consequence, two-phonon Raman spectroscopy is sensitive to the dynamics of the photoexcited electron-hole (e-h) pairs, i.e., other than e-ph inelastic-scattering processes they can undergo, for example, e-e collisions.[18] Assuming that these two processes are the main scattering mechanisms, the integrated intensities over the full linewidth of the $2D$ and $2D'$ Raman peaks, which represent the probabilities of the respective Raman processes, can be expressed as[19]

$$A(2D) = 2C(\gamma_K/\gamma)^2, \tag{1a}$$

$$A(2D') = C(\gamma_\Gamma/\gamma)^2, \tag{1b}$$

where C is a constant and 2γ denotes the inelastic-scattering rate of the photoexcited e-h pair written as

$$\gamma = \gamma_{e\text{-}ph} + \gamma_{e\text{-}e} \tag{2}$$

and the phonon emission rate $\gamma_{e\text{-}ph}$ includes phonons near $\mathbf{\Gamma}$ and $\mathbf{K}$,

$$\gamma_{e\text{-}ph} = \gamma_{\Gamma} + \gamma_{K}. \tag{3}$$

The increased, if any, presence of disorder in the graphene surface after ozone treatment is not enough to have an impact on Raman spectra, in view of the undetectable presence of D and D' peaks in the spectrum of the pristine [cf. Fig. 2(a)(loop 0)] and ozone exposed graphene sheet [cf. Fig. 2(a) (loop 1–3)]. Consequently, competing elastic processes by defects are disregarded.

Since the e-e scattering is dependent on carrier density, both $2D$ and $2D'$ intensities are sensitive to doping level. The e-e scattering rate, $2\gamma_{e\text{-}e}$, was found[20] to be proportional to the Fermi energy, E_F, and up to first order in E_F it is expressed as

$$\gamma_{e\text{-}e} = |E_F| f, \tag{4}$$

where the proportionality coefficient f depends on the Coulomb coupling constant. The intensity of the G peak should not depend on doping since the given Raman process is in off-resonance condition.[19] Therefore, the Raman peak intensity variation shown in Fig. 2, i.e., decrease in two-phonon Raman peaks intensity and unchanged G peak intensity, could be attributed to a change in the carrier concentration due to ozone treatment.

B. Frequency shift of Raman bands

The above interpretation is reinforced by monitoring the changes in frequency of the Raman spectrum feature after each ozone cycle, given the extensively reported dependence of the Raman modes frequency on doping in graphene. Charge-transfer modification of the chemical-bond induces variations in bond lengths (stiffening/softening), reflected in the variation in the phonon frequency. It has been shown that in graphene this effect alone does not explain the behavior of the Raman peaks frequency with doping, and therefore effects arising from the suppression of the Kohn anomaly at $\mathbf{\Gamma}$ and $\mathbf{K}$ points must be invoked.[2,35]

The G peak frequency increases for both n and p doping, due to the nonadiabatic removal of the Kohn anomaly from the $\mathbf{\Gamma}$ point.[7,8] Anomalous phonon softening, which is seen at low temperature but is smeared at 300 K, reflects a resonant e-ph coupling effect when the e-h energy gap is smaller than the phonon energy.[10] Moreover, when the e-h energy gap reaches a value higher than the phonon energy a sharp linewidth reduction occurs as the phonon decay process into e-h pairs suddenly ceases.[7,8]

The $2D$ peak shows a different dependence on doping, which helps discerning between n- and p-type doping.[9,11] For electron doping, the $2D$ peak frequency does not change much until a high electron concentration is reached, showing a softening for further increase. For hole doping, the frequency of the $2D$ peak increases at a rate higher than solely expected from variations in lattice spacing.[9,11] Although phonon modes contributing to $2D$ peak are away from $\mathbf{K}$ points, the effects of the Kohn anomaly are not negligible due to the strong e-ph coupling.[36,37] As the doping level increases, the Kohn anomaly close to $\mathbf{K}$ points is smeared out contributing to the stiffening of the $2D$ peak. However, a complete understanding of the response of the $2D$ band to doping is still missing and it would benefit from the inclusion in the theory of nonlocal electron exchange-correlation effects. In contrast, the influence of the Kohn anomaly at $\mathbf{\Gamma}$ becomes weaker as the phonon wave vector departs from this point.[38] Therefore, the $2D'$ peak frequency is expected to be almost insensitive to changes in doping level, beyond the dependence on the lattice spacing variation.[2,35]

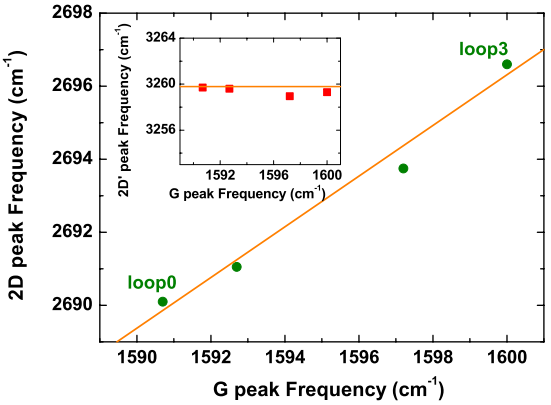

FIG. 3. (Color online) Frequency shifts of the Raman $2D$ vs G peak obtained after each ozone exposure cycle. The inset shows the evolution of the Raman $2D'$ vs G peak frequency.

Finally, charge concentration changes are not the only possible source of phonon spectrum variation. Strain effects have already been measured in the Raman spectrum of graphene.[39] The splitting of the G band into two components displays a shift with applied uniaxial strain at a rate of 11 and 32 $\text{cm}^{-1}/\%$. The $2D$ and $2D'$ bands do not split and they show a shift amounting to 64 $\text{cm}^{-1}/\%$ and 35 $\text{cm}^{-1}/\%$, respectively.

Figure 3 displays the Raman G and $2D$ peak frequencies showing a blueshift with increasing exposure to ozone. The Raman $2D'$ peak position, on the contrary, displays no variation within the experimental resolution (see inset to Fig. 3). The larger frequency variation in the G peak compared to the $2D$ peak, together with a constant $2D'$ peak frequency, rules out the effect of strain. Therefore, we conclude that the graphene surface increases its p doping level with each ozone exposure cycle. The present method to change the amount of doping does not require additional processing to fabricate contacts, which can affect the crystal quality and the homogeneity of the properties of the graphene flakes. Comparing the measured phonons frequency shift in the present study with those found in the literature, we obtain the overall change in the carrier concentration to be $\Delta p_{tot} \approx 5 \times 10^{12}$ cm^{-2}. The Raman spectrum after four ozone exposure cycles (not displayed) shows no further changes, neither in the two-phonon peak intensities nor in the peak position of the G and $2D$ features, indicating that the charge concentration, i.e., the ozone adsorption, reached a constant value.

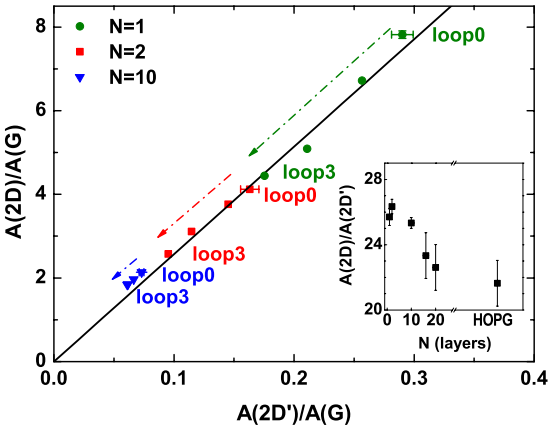

FIG. 4. (Color online) Experimental $A(2D)/A(G)$ vs $A(2D')/A(G)$ Raman peaks area ratio from single-layer graphene (solid circles), double-layer graphene (solid squares) and ten-layer graphene (solid triangles) spectra measured before ozone treatment and after each ozone exposure cycle. The inset shows the $A(2D)/A(2D')$ ratio as a function of the number of graphene layers, N.

C. Electron-phonon coupling parameters ratio

Figure 4 (solid circles) shows the integrated intensity of the $2D$ peak, $A(2D)$, as a function of the integrated intensity of the $2D'$ peak, $A(2D')$, both normalized to the integrated intensity of the G peak, $A(G)$, calculated from spectra of Fig. 2. This dependence, besides showing the common decrease in the intensity values, as expected from Fig. 2, unveils a constant $A(2D)/A(2D')$ ratio, as they closely follow a straight line. The decrease in intensity is a direct consequence of the increase in $\gamma_{e\text{-}e}$ with doping [cf. Eqs. (1a) and (1b)]. On the contrary, the constant $A(2D)/A(2D')$ ratio indicates a weaker dependence of $\gamma_{e\text{-}ph}$ on doping. This point becomes clear taking the ratio of Eqs. (1a) and (1b), which is found to be proportional to the square of the emission rates ratio of E_g and A_1 phonons,

$$A(2D)/A(2D') = 2(\gamma_K/\gamma_\Gamma)^2. \tag{5}$$

The linear fit to the single-layer data in Fig. 4 gives a value of the slope of $26 \pm 3\%$ and, from Eq. (5), we then obtain the ratio of phonon emission rates, $\gamma_K/\gamma_\Gamma = 3.6$. This ratio is related to the adimensional EPC parameters λ_Γ and λ_K, as defined in Ref. 19, according to

$$\frac{\gamma_K}{\gamma_\Gamma} = \frac{\omega_{out,K}}{\omega_{out,\Gamma}} \frac{\lambda_K}{\lambda_\Gamma}, \tag{6}$$

where $\omega_{out,\Gamma} = E_L - 2\omega_\Gamma$ and $\omega_{out,K} = E_L - 2\omega_K$ are the frequencies of the emitted photons (E_L is the frequency of the incident photons) in the respective Raman processes involving phonons at $\mathbf{\Gamma}$ and $\mathbf{K}$ point, with frequencies ω_Γ and ω_K, respectively. In order to compare with available calculated and experimental values, we relate the EPCs parameters to the square of the *e-ph* interaction matrix elements averaged on the Fermi surface, $\langle D_\Gamma^2 \rangle_F$ and $\langle D_K^2 \rangle_F$, as follows:[20,40]

$$\frac{\lambda_K}{\lambda_\Gamma} = \frac{\omega_\Gamma}{\omega_K} \frac{\langle D_K^2 \rangle_F}{2\langle D_\Gamma^2 \rangle_F}. \tag{7}$$

While the value of $\langle D_K^2 \rangle_F$ of graphene and related graphitic structures has been controversial, due to the lack of reliable experimental data of the phonon dispersion around the $\mathbf{K}$ point, until recently,[37] the value of $\langle D_\Gamma^2 \rangle_F$ was obtained[41] by relating it to the measured dispersion of the E_g mode near $\mathbf{\Gamma}$.[38] Then taking $\langle D_\Gamma^2 \rangle_F = 39$ $(\text{eV}/\text{Å})^2$, from Eqs. (6) and (7) we obtain $\langle D_K^2 \rangle_F = 205$ $(\text{eV}/\text{Å})^2$. The latter is close to the EPC value found experimentally from the phonon dispersion around the $\mathbf{K}$ point of graphite,[37] and to the computed EPC values of graphene and graphite, when nonlocal exchange-correlation effects are included.[36] Actually, $\langle D_K^2 \rangle_F$ of graphene and graphite are expected to differ slightly due to a large screening effect of the exchange interaction in the latter. We measured the $A(2D)/A(2D')$ ratio in HOPG and found a value about 20% lower than in graphene (cf. inset to Fig. 4). For samples with thicknesses of around twenty graphene layers the values of the $A(2D)/A(2D')$ ratio are midway between graphene and graphite. The value of $\langle D_K^2 \rangle_F$ is then found to be in the range of 205–188 $(\text{eV}/\text{Å})^2$.

Finally, concerning the doping dependence of EPC parameters in graphene, it has been calculated that $\langle D_K^2 \rangle_F$ reduces by $\approx 16\%$ for a variation in $\Delta p = 1.9 \times 10^{13}$ cm^{-2} while $\langle D_\Gamma^2 \rangle_F$ remains unaffected.[42] Taking into account that our estimated Δp_{tot} is about four times smaller, the expected decrease in $\langle D_K^2 \rangle_F$ stays within the experimental error. A similar argument can be given to exclude any significant effect of the electron velocity, v_F, with doping on the two-phonon Raman intensities. The latter are related to v_F in Eqs. (1a) and (1b) as follows:[19,20]

$$C = \frac{4}{3}\left(\frac{e^2}{c}\right)^2 \frac{v_F^2}{c^2}, \tag{8}$$

where c is the speed of light and e the electron charge. The estimate of the v_F change for variations in p found in the present study[43] supports the assumption of a constant C value.

D. Electron-electron coupling and number of graphene layers

In Fig. 4, we included data of Raman measurements from bilayer (BL) and ten-layer (TL) graphene deposited on the same SiO_2/Si wafer as the monolayer sample, solid squares and triangles, respectively. The experimental Raman intensities show a good correlation with the monolayer data, as they closely follow the linear relation with slope value of 26 (thick line in Fig. 4). A significant feature is the decrease in the intensity rate change, given by the difference between intensities in successive treatment loops, which is seen as a higher concentration of data points in Fig. 4, when comparing single-layer (SL), bilayer, and ten-layer samples. The dotted-dashed line arrows in Fig. 4 are plotted to illustrate the data contraction with increasing number of layers, which is found to be related by the ratio $\Delta A(2D)_{\text{SL}} \approx 2\Delta A(2D)_{\text{BL}} \approx 10\Delta A(2D)_{\text{TL}}$, within an error of approximately 10%. Since, as discussed previously, the decrease in $A(2D)$ and $A(2D')$, that follows ozone treatment, is related to the in-

crease in hole concentration, the result of Fig. 4 suggests that the rate of decrease in the intensity, $\Delta A(2D)$ [$\Delta A(2D')$], with doping becomes smaller by a factor inversely proportional to the number of graphene layers.

In order to understand the relation $\Delta A(2D) \propto N^{-1}$ [$\Delta A(2D') \propto N^{-1}$], we first recall that a Bernal stack with N layers, N even [N odd], has $N/2$ [$(N+1)/2$] electronlike and $N/2$ [$(N+1)/2$] holelike subbands almost touching at the **K** point with a band overlap smaller than 41 meV. Additional $N/2$ [$(N-1)/2$] electronlike and $N/2$ [$(N-1)/2$] holelike outer subbands appear with decreasing energy separation with layer number, reaching a maximum value of 0.4 eV in bilayer graphene. The outermost subband is found in the range from 0.4 eV in bilayer to ≈0.8 eV for 20 graphene layers.[44] As the number of layers increases, the number of *e-ph* processes that contributes to the $2D$ ($2D'$) integrated intensity also grows and it is determined by the selection rules for optical excitations and for electron scattering by phonons.[45] Since the integrated intensities contain the weighted probability of the different processes involving phonons with close wave vector, the $A(2D)/A(2D')$ ratio only depends on the EPC parameters which, up to ten layers, remain constant as inferred from the lineal relation of the data in Fig. 4. The $\gamma_{e\text{-}e}$ scattering rate, on the other hand, experiences an increase as the intersubband *e-e* collisions are allowed, following the appearance of more subbands with increasing number of layers. Although for the E_F range studied in the present work the parabolicity of the energy subbands should be taken into account, for illustrative purposes the high doping case is considered where the energy dispersion of the subbands can be taken as linear.[11,46] Then, in the approximation of small momentum transfer, we can generalize Eq. (4) to N layers as, $\gamma_{e\text{-}e}=N|E_F|f$. Considering linear dispersive subbands, the carrier concentration, p, is given by $p=N\mu E_F^2$. For highly doped samples, the contribution from *e-ph* scattering to the total scattering rate can be neglected compared to the much bigger *e-e* scattering component. Thus, the integrated intensity for multilayer graphene can be written as

$$A(2D)_{NL} \approx 2C\frac{\gamma_K^2}{N^2 f^2 \frac{p}{N}} \tag{9}$$

and its rate of decrease upon the change in the carrier concentration, Δp, is

$$\frac{\Delta A(2D)}{\Delta p} = -2C\frac{\gamma_K^2}{N f^2 p^2}, \tag{10}$$

which accounts for the contraction of the data in Fig. 4 with increasing number of layers.

Based on Eq. (10), the approximate dependence of the experimental two-phonon Raman intensity with the inverse of N proves that the amount of initial, p, and transferred, Δp, charge concentration in the different samples, SL graphene, BL graphene, and TL graphene, ought to be similar. Taking into account that all samples were placed on the same wafer and exposed to the same treatments, it is reasonable to assume that the extent of unintentional or background doping and adsorbate coverage was comparable among them. The dependence of the two-phonon integrated intensity on the number of layers is twofold, as seen from Eq. (9). First, the charge concentration is distributed among the subbands, the number of which increase with the number of layers, leading to a decrease in the probability of *e-e* collision. Second, with increasing number of subbands the number of allowed *e-e* processes also increases and, with it, the probability of *e-e* collision. Nevertheless, the overall effect is a decrease in the two-phonon Raman intensity because there is the contribution in the scattering rate from the simultaneously excited electron and hole, as the square in Eq. (1a) reflects.

IV. CONCLUSIONS

In conclusion, we have shown that the carrier concentration in graphene gradually increases with sequential ozone short-exposure cycles while preserving its crystallinity. The blueshift of the G and $2D$ peak frequencies is evidence of p doping of the samples. In contrast to the G peak intensity, which is found to remain constant, the $2D$ and $2D'$ peak intensities decrease with increasing number of ozone exposure cycles, i.e., with increasing doping. This effect reflects the responsiveness of the two-phonon Raman intensity to the dynamics of photoexcited *e-h* pairs and, in particular, to the contribution of the *e-e* scattering. We used this dependence to extract the EPC of phonons near the **K** point and found a close agreement with previous experimental and theoretical values. We also demonstrated an inverse dependence of the rate of decrease in the intensities upon doping on the graphene number of layers, reflecting the increased probability of *e-e* scattering with increasing number of layers.

ACKNOWLEDGMENTS

We are grateful to M. Lira-Cantú for the use of the ozone chamber. Support from the Spanish Ministry of Science and Innovation (Projects No. FIS2008-06830 and No. FIS2009-10150) and the EU project NANOPACK (Project No 216176) is gratefully acknowledged.

*francesc.alsina.icn@uab.cat

†Present address: RIMNST, Jiao Tong University, 200240, Shanghai, China.

[1] T. Ando, J. Phys. Soc. Jpn. **75**, 124701 (2006).

[2] M. Lazzeri and F. Mauri, Phys. Rev. Lett. **97**, 266407 (2006).

[3] G. G. Samsonidze, E. B. Barros, R. Saito, J. Jiang, G. Dresselhaus, and M. S. Dresselhaus, Phys. Rev. B **75**, 155420 (2007).

[4] K. S. Novoselov, A. Geim, S. Morozov, D. Jiang, Y. Zhang, S. Dubonos, I. Grigorieva, and A. Firsov, Science **306**, 666 (2004).

[5] K. S. Subrahmanyam, R. Voggu, A. Govindaraj, and C. N. R.

Rao, Chem. Phys. Lett. **472**, 96 (2009).
[6] N. Jung, N. Kim, S. Jockusch, N. J. Turro, P. Kim, and L. Brus, Nano Lett. **9**, 4133 (2009).
[7] S. Pisana, M. Lazzeri, C. Casiraghi, K. S. Novoselov, A. K. Geim, A. C. Ferrari, and F. Mauri, Nature Mater. **6**, 198 (2007).
[8] J. Yan, Y. Zhang, P. Kim, and A. Pinczuk, Phys. Rev. Lett. **98**, 166802 (2007).
[9] A. Das, B. Chakraborty, S. Piscanec, S. K. Saha, U. V. Waghmare, K. S. Novoselov, H. R. Krishnamurthy, A. K. Geim, A. C. Ferrari, and A. K. Sood, Nat. Nanotechnol. **3**, 210 (2008).
[10] J. Yan, E. A. Henriksen, P. Kim, and A. Pinczuk, Phys. Rev. Lett. **101**, 136804 (2008).
[11] A. Das, B. Chakraborty, S. Piscanec, S. Pisana, A. K. Sood, and A. C. Ferrari, Phys. Rev. B **79**, 155417 (2009).
[12] C. Stampfer, F. Molitor, D. Graf, K. Ensslin, A. Jungen, C. Hierold, and L. Wirtz, Appl. Phys. Lett. **91**, 241907 (2007).
[13] M. Hulman, M. Haluska, G. Scalia, D. Obergfell, and S. Roth, Nano Lett. **8**, 3594 (2008).
[14] S. Berciaud, S. Ryu, L. E. Brus, and T. F. Heinz, Nano Lett. **9**, 346 (2009).
[15] Y. Shi, X. Dong, P. Chen, J. Wang, and L.-J. Li, Phys. Rev. B **79**, 115402 (2009).
[16] C. Casiraghi, S. Pisana, K. S. Novoselov, A. K. Geim, and A. C. Ferrari, Appl. Phys. Lett. **91**, 233108 (2007).
[17] Z. H. Ni, T. Yu, Z. Q. Luo, Y. Y. Wang, L. Liu, C. P. Wong, J. Miao, W. Huang, and Z. X. Shen, ACS Nano **3**, 569 (2009).
[18] D. M. Basko, Phys. Rev. B **76**, 081405(R) (2007).
[19] D. M. Basko, Phys. Rev. B **78**, 125418 (2008).
[20] D. M. Basko, S. Piscanec, and A. C. Ferrari, Phys. Rev. B **80**, 165413 (2009).
[21] C. Casiraghi, Phys. Rev. B **80**, 233407 (2009).
[22] A. Tracz, G. Wegner, and J. P. Rabe, Langmuir **19**, 6807 (2003).
[23] G. Lee, B. Lee, J. Kim, and K. Cho, J. Phys. Chem. C **113**, 14225 (2009).
[24] W.-L. Yim and J. K. Johnson, J. Phys. Chem. C **113**, 17636 (2009).
[25] S. Picozzi, S. Santucci, L. Lozzi, C. Cantalini, C. Baratto, G. Sberveglieri, I. Armentano, J. M. Kenny, L. Valentini, and B. Delley, J. Vac. Sci. Technol. A **22**, 1466 (2004).
[26] R. Ma, D. Yoon, K.-Y. Chun, and S. Baik, Chem. Phys. Lett. **474**, 158 (2009).
[27] H. Tao, J. Moser, F. Alzina, A. Bachtold, and C. M. Sotomayor-Torres, (unpublished).
[28] B. Krauss, T. Lohmann, D. H. Chae, M. Haluska, K. von Klitzing, and J. H. Smet, Phys. Rev. B **79**, 165428 (2009).
[29] The number of layers in graphene can be determined from the capability of graphene to absorb a significant fraction of the incident light with each added layer (Ref. 47). The rate of absorption with the number of layers was obtained from the decrease in the Raman peak of silicon located underneath the graphene flakes and the silicon oxide film.
[30] F. Tuinstra and J. L. Koenig, J. Chem. Phys. **53**, 1126 (1970); R. J. Nemanich and S. A. Solin, Phys. Rev. B **20**, 392 (1979); Y. Kawashima and G. Katagiri, *ibid.* **52**, 10053 (1995); A. C. Ferrari and J. Robertson, *ibid.* **61**, 14095 (2000); C. Thomsen and S. Reich, Phys. Rev. Lett. **85**, 5214 (2000).
[31] S. Reich and C. Thomsen, Philos. Trans. R. Soc. London, Ser. A **362**, 2271 (2004).
[32] A. C. Ferrari, Solid State Commun. **143**, 47 (2007).
[33] M. Lucchese, F. Stavale, E. Martins Ferreira, C. Vilani, M. Moutinho, R. B. Capaz, C. Achete, and A. Jorio, Carbon **48**, 1592 (2010).
[34] J. C. Charlier, P. C. Eklund, J. Zhu, and A. C. Ferrari, in *Carbon Nanotubes*, Topics in Applied Physics Vol. 111 (Springer-Verlag, Berlin, 2008), Chap. 8, pp. 673–709.
[35] S. K. Saha, U. V. Waghmare, H. R. Krishnamurthy, and A. K. Sood, Phys. Rev. B **76**, 201404(R) (2007).
[36] M. Lazzeri, C. Attaccalite, L. Wirtz, and F. Mauri, Phys. Rev. B **78**, 081406(R) (2008).
[37] A. Grüneis, J. Serrano, A. Bosak, M. Lazzeri, S. L. Molodtsov, L. Wirtz, C. Attaccalite, M. Krisch, A. Rubio, F. Mauri, and T. Pichler, Phys. Rev. B **80**, 085423 (2009).
[38] J. Maultzsch, S. Reich, C. Thomsen, H. Requardt, and P. Ordejón, Phys. Rev. Lett. **92**, 075501 (2004).
[39] T. M. G. Mohiuddin, A. Lombardo, R. R. Nair, A. Bonetti, G. Savini, R. Jalil, N. Bonini, D. M. Basko, C. Galiotis, N. Marzari, K. S. Novoselov, A. K. Geim, and A. C. Ferrari, Phys. Rev. B **79**, 205433 (2009).
[40] M. Calandra and F. Mauri, Phys. Rev. B **76**, 205411 (2007).
[41] M. Lazzeri, S. Piscanec, F. Mauri, A. C. Ferrari, and J. Robertson, Phys. Rev. B **73**, 155426 (2006).
[42] C. Attaccalite, L. Wirtz, M. Lazzeri, F. Mauri, and A. Rubio, Nano Lett. **10**, 1172 (2010).
[43] C. Attaccalite and A. Rubio, Phys. Status Solidi B **246**, 2523 (2009).
[44] B. Partoens and F. M. Peeters, Phys. Rev. B **74**, 075404 (2006).
[45] L. M. Malard, M. H. D. Guimarães, D. L. Mafra, M. S. C. Mazzoni, and A. Jorio, Phys. Rev. B **79**, 125426 (2009).
[46] T. Ando, J. Phys. Soc. Jpn. **76**, 104711 (2007).
[47] R. R. Nair, P. Blake, A. N. Grigorenko, K. S. Novoselov, T. J. Booth, T. Stauber, N. M. R. Peres, and A. K. Geim, Science **320**, 1308 (2008).